XIII International Conference on Computational Plasticity. Fundamentals and Applications
COMPLAS XIII
E. Oñate, D.R.J. Owen, D. Peric & M. Chiumenti (Eds)

NON-LINEAR STATIC ANALYSIS OF MASONRY STRUCTURES

JONAS COENE, STIJN FRANÇOIS AND GEERT DEGRANDE

Department of Civil Engineering, KU Leuven
Kasteelpark Arenberg 40, 3001 Leuven, Belgium
e-mail: jonas.coene@bwk.kuleuven.be

Key words: Masonry, Non-linear Interface Element, Dissipation Based Arc-length Method

Abstract. A meso-scale model is used to model a masonry structure where bricks are modelled using finite volume elements and mortar joints are modelled using finite interface elements. A plasticity based cohesive zone model is used for the interfaces as cracks mainly propagate at the mortar joints. To avoid numerical problems associated with snapbacks observed in experiments on masonry walls, a dissipation based arc-length method is used to trace the static equilibrium path. Finally, a numerical simulation of a shear test on a 2×1.5 brick wall is performed.

1 INTRODUCTION

Vibration induced damage to structures due to sources of low to moderate amplitude, such as road traffic and construction activities, is a common concern. Damage can be classified as direct damage due to an excessive response of structural members in the case of moderate amplitude vibrations, such as construction activities, or as damage due to long term exposure to low amplitude vibrations, such as road traffic, which can result in fatigue damage or foundation settlements. The versatility of damage mechanisms makes it difficult to establish general limit values for vibration related damage and motivates a numerical investigation of the mechanical behaviour of brittle construction materials.

For the modelling of the constitutive behaviour of masonry, a homogenized criterion is often used [1], where the constitutive relations are described on the macro-scale. However, for a non-linear orthotropic composite such as masonry, the representation of full damage induced anisotropy remains complex and involves difficult parameter identification procedures.

The limitations of homogenized models for masonry have motivated the development of meso-scale models [2, 3], where more straightforward constitutive laws are formulated on the mesoscopic scale. A popular approach is to use finite volume elements for the bricks and finite interface elements for the joints [4]. As the possible crack locations are

mainly located at the mortar joint, a plasticity based cohesive zone model is used for the interface elements [4, 5]. To improve the efficiency, these meso-scale models can be incorparated in a multi-scale approach [6].

Because of the brittle nature of masonry, special attention has to be paid to the global solution strategy. Macorini et al. [4, 7] use a dynamic analysis to avoid numerical problems associated with the sudden release of elastic energy when cracks propogate in the masonry. The stability of these methods strongly depends the damping and mass matrices. In order to assess the effect of soil settlement, a static solution method can be used. Therefore, an arc-length method is often used [8]. However, for many materially non-linear problems the global norms used in these methods are inappropriate and a different constraint equation has to be used. Verhoosel et al. [9] proposed a dissipation based arc-length method. The constraint equation is based on the rate of energy dissipation which is equal to the exerted power minus the rate of elastic energy. This method is only applicable for dissipative parts of the equilibrium path. A second alternative is an adaptive path following scheme [10] where, for every load increment, a control region is identified where control parameters in the constraint equation are evaluated. This region changes with the propagation of damage.

In this paper, the meso-scale model for masonry proposed by Macorini et al. [4] is used. In the first section the mesoscale model and the constitutive behaviour of the interface element are covered in more detail. To obtain a global solution, a dissipation based arc-length method is used [9]. In the last section, two numerical examples on a single interface element and a direct shear test on a small brick assembly are performed.

2 MESOSCALE MODEL FOR MASONRY

The 3D meso-scale model proposed by Macorini et al. [4] is used. Bricks are modelled using linear elastic finite volume elements and mortar joints are modelled with two-dimensional interface elements. Additionally, interface elements are added in the vertical mid-plane of the bricks to account for possible failure of the units (figure 1). Linear elastic material behaviour is assumed for the solid elements, whereas the 2D interface elements account for the material nonlinearity of masonry as cracks propogate most often in the mortar joints [4, 7]. This methodology allows to model structural details at the meso-scale, properly accounting for interaction of the masonry with other structural parts such as lintels at windows and door openings.

2.1 Interface model

An interface element consists of two faces corresponding either to the faces of two solid elements bound through a mortar layer or to adjacent faces of solid elements for a single brick. Initially, the two faces are coincident. An elasto-plastic contact law based on a Mohr-Coulomb criterion is used to model failure in tension and shear. The material model is defined within the framework of plasticity [11], taking into account the softening

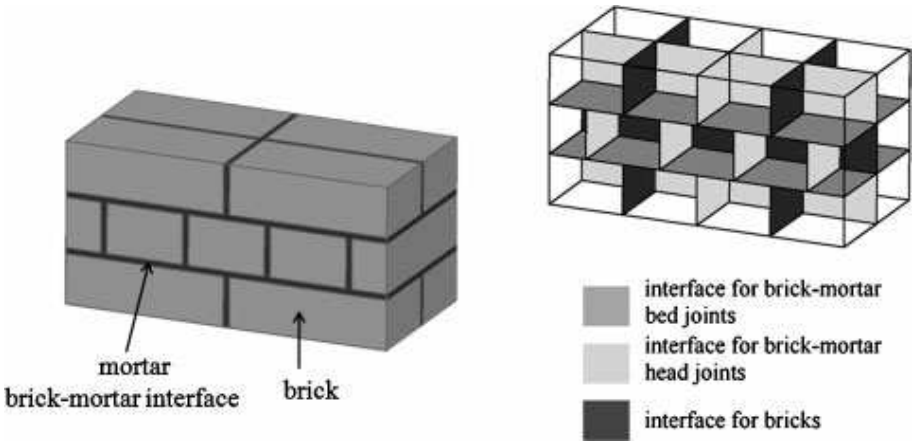

Figure 1: Mesoscale model of masonry using solid elements and non-linear interface elements [4].

behaviour of masonry [11].

The local material model is formulated in terms of tractions and relative displacements of the two faces of the interface element. A local frame of reference is defined where the x- and y-axis lie in the plane of the interface element and the z-axis is normal to the plane as shown in figure 2a. The traction vector and relative displacement vector are $\mathbf{t} = \{t_x, t_y, t_z\}^{\mathrm{T}}$ and $\mathbf{u}^{\mathrm{r}} = \{u_x^{\mathrm{r}}, u_y^{\mathrm{r}}, u_z^{\mathrm{r}}\}^{\mathrm{T}}$. Once the interface starts yielding, the incremental relative displacement vector can be decomposed into an elastic and a plastic part:

$$d\mathbf{u}^{\mathrm{r}} = d\mathbf{u}^{\mathrm{e}} + d\mathbf{u}^{\mathrm{p}} \tag{1}$$

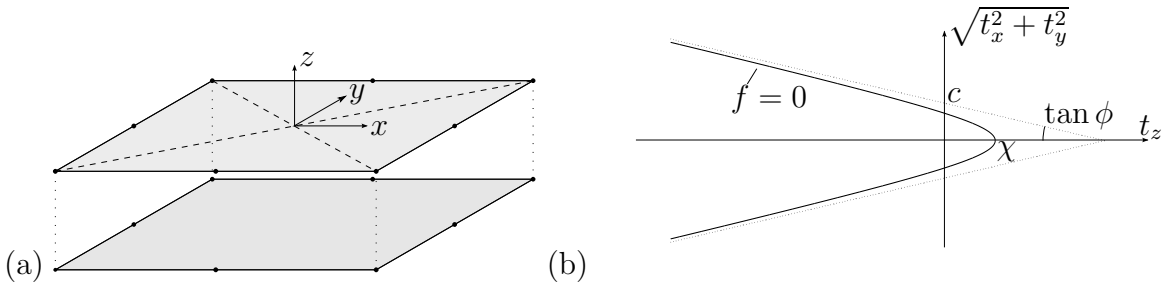

Figure 2: (a) Local frame of reference and (b) hyperbolic yield surface for the interface element.

A hyperbolic yield surface is adopted (figure 2b) which has a smooth transition from the Mohr-Coulomb criterium under compression to tension cut-off under pure tension [12, 13], so that numerical problems associated with the Mohr-Coulomb cone are avoided. The yield surface is defined by the tensile strength χ, cohesion c and friction angle ϕ of the interface material:

$$f = -(c - t_z \tan\phi) + \sqrt{t_x^2 + t_y^2 + (c - \chi \tan\phi)^2} = 0 \tag{2}$$

The evolution of the yield surface is controlled by the history variable W^{p} which is a measure for the work done during the fracture process [3]. The increment of the history variable is given by:

$$dW^{\mathrm{p}} = \begin{cases} \mathbf{t} d\mathbf{u}^{\mathrm{p}} & \text{if} \quad t_z \geq 0 \quad \text{(tension)} \\ \left(\sqrt{t_x^2 + t_y^2} + t_z \tan\phi\right) \sqrt{\left(du_x^{\mathrm{p}}\right)^2 + \left(du_y^{\mathrm{p}}\right)^2} & \text{if} \quad t_z < 0 \quad \text{(compression)} \end{cases} \tag{3}$$

In tension, all dissipated plastic work is used to form a tensile crack. In compression, however, the total dissipated work also includes heat production due to friction which does not contribute to crack formation. This is accounted for in W^{p} by the second term $t_z \tan\phi$. The evolution of the tensile strength, cohesion and friction angle is respectively given by [3]:

$$\begin{aligned} \chi &= \chi_0(1 - \xi_{\mathrm{I}}) \\ c &= c_0(1 - \xi_{\mathrm{II}}) \\ \tan\phi &= \tan\phi_0 - (\tan\phi_0 + \tan\phi_{\mathrm{r}})\xi_{\mathrm{II}} \end{aligned} \tag{4}$$

where χ_0, c_0 and ϕ_0 are initial values and ϕ_{r} is the residual friction angle. ξ_{I} and ξ_{II} are two non-dimensional variables defined by:

$$\xi_i = \begin{cases} \frac{1}{2} - \frac{1}{2}\cos\left\{\frac{\pi W^{\mathrm{p}}}{G_{\mathrm{f}}^i}\right\}, & 0 \leq W^{\mathrm{p}} \leq G_{\mathrm{f}}^i \\ 1, & W^{\mathrm{p}} > G_{\mathrm{f}}^i \end{cases} \quad \text{with} \quad i = \mathrm{I}, \mathrm{II} \tag{5}$$

$G_{\mathrm{f}}^{\mathrm{I}}$ represents the fracture energy for mode I failure (tension) and $G_{\mathrm{f}}^{\mathrm{II}}$ represents the fracture energy for mode II failure (shear).

2.2 Elasto-plastic relation

Starting from equation (1), a relation between incremental displacements and tractions is derived. The elastic part of the displacement increment is obtained from:

$$d\mathbf{t} = \begin{bmatrix} k_{\mathrm{n}} & 0 & 0 \\ 0 & k_{\mathrm{t}} & 0 \\ 0 & 0 & k_{\mathrm{t}} \end{bmatrix} = \mathbf{K}^{\mathrm{e}} d\mathbf{u}^{\mathrm{e}} \tag{6}$$

where the normal and tangential stiffness k_{n} and k_{t} depend on the elastic properties and dimensions of the mortar joint. It is assumed that the normal and tangential stiffness are decoupled [7].

The plastic displacement increment $d\mathbf{u}^{\mathrm{p}}$ is derived from a plastic potential g:

$$d\mathbf{u}^{\mathrm{p}} = d\lambda \frac{\partial g}{\partial \mathbf{t}} \tag{7}$$

where $d\lambda$ is an inelastic multiplier. For a brittle material like masonry, a non-associative flow rule is used to account for the dilatancy of the fracture surface [3]. A hyperbolic surface simular to the yield surface is used:

$$g = -(c_g - t_z \tan\phi_g) + \sqrt{t_x^2 + t_y^2 + (c_g - \chi \tan\phi_g)^2} = 0 \tag{8}$$

with different values c_g and ϕ_g for the cohesion and friction angle, while the tensile strength χ is the same as for the yield surface.

The traction increment can now be written as:

$$d\mathbf{t} = \mathbf{K}^{\mathrm{e}} d\mathbf{u}^{\mathrm{r}} - d\lambda \mathbf{K}^{\mathrm{e}} \frac{\partial g}{\partial \mathbf{t}} \tag{9}$$

Plastic deformations can only occur as long as the traction point is located on the yield surface which is imposed by the consistency condition [13]:

$$\frac{\partial f}{\partial \mathbf{t}} d\mathbf{t} + \frac{\partial f}{\partial \mathbf{u}^{\mathrm{p}}} d\mathbf{u}^{\mathrm{p}} = 0 \tag{10}$$

Substituting expression (9) and solving for $d\lambda$ yields:

$$d\lambda = \frac{\frac{\partial f}{\partial \mathbf{t}} \mathbf{K}^{\mathrm{e}} d\mathbf{u}^{\mathrm{r}}}{\frac{\partial f}{\partial \mathbf{t}} \mathbf{K}^{\mathrm{e}} \frac{\partial g}{\partial \mathbf{t}} - \frac{\partial f}{\partial \mathbf{u}^{\mathrm{p}}} d\mathbf{u}^{\mathrm{p}}} \tag{11}$$

Finally, the traction increment is obtained as:

$$d\mathbf{t} = \left(\mathbf{K}^{\mathrm{e}} - \frac{\mathbf{K}^{\mathrm{e}} \frac{\partial f}{\partial \mathbf{t}} \frac{\partial g}{\partial \mathbf{t}}}{\mathbf{K}^{\mathrm{e}} \frac{\partial g}{\partial \mathbf{t}} \frac{\partial g}{\partial \mathbf{t}} - \frac{\partial f}{\partial \mathbf{u}^{\mathrm{p}}} d\mathbf{u}^{\mathrm{p}}} \right) d\mathbf{u}^{\mathrm{r}} = \mathbf{K}^{\mathrm{ep}} d\mathbf{u}^{\mathrm{r}} \tag{12}$$

where $\mathbf{K}^{\mathrm{ep}}$ is the elasto-plastic stiffness matrix.

In a finite element context, a return mapping algorithm is used to obtain the traction increment for a certain displacement increment since the elasto-plastic stiffness matrix depends on the final traction state which is initially unknown [11]. At the end of the iterative process, the consistent tangent stiffness matrix is obtained as the first derivative of the tractions with respect to the relative displacements [3, 4]:

$$\mathbf{K}^{\mathrm{t}} = \frac{\partial \mathbf{t}}{\partial \mathbf{u}^{\mathrm{r}}} \tag{13}$$

Furthermore, a substepping algorithm is adopted to improve accuracy and robustness of the local iteration [4].

3 GLOBAL SOLUTION STRATEGY

The non-linear interface element is implemented in the finite element toolbox StaBIL [14] in Matlab. Both static and dynamic solution strategies can be used to trace the equilibrium path. However, when cracks propagate along the structure, the elastic energy stored in the bulk material connected to a damaged interface has to be redistributed into other elements, leading to possible snapbacks in the global solution and numerical instabilities [4]. Therefore, a dissipation based arc-length method is employed [9, 15] where the arc-length constraint is based on the energy release rate, which has the advantage that it is directly related to the failure process.

3.1 Dissipation based arc-length method

The dissispation based arc-length method presented by Verhoosel et al. [9] is used. The basic equations of the method and constraint equation adapted for the interface element are discussed below.

A body is in equilibrium if the internal forces are equal to the external forces:

$$\mathbf{f}_{\text{int}}(\mathbf{u}) = \mathbf{f}_{\text{ext}} = \lambda \mathbf{f} \tag{14}$$

The internal forces $\mathbf{f}_{\text{int}}$ are a function of the displacements $\mathbf{u}$. The external forces $\mathbf{f}_{\text{ext}}$ can be expressed as a unit force vector $\mathbf{f}$ multiplied by a load factor λ. A collection of points $(\mathbf{u}, \lambda)$ that satisfy equation (14) form an equilibrium path. Given an initial equilibrium point $(\mathbf{u}_0, \lambda_0)$, the next point on the equilibrium path can be found by solving the following system of equations for the incremental displacement $\Delta\mathbf{u}$ and the incremental load factor $\Delta\lambda$:

$$\mathbf{f}_{\text{int}}(\mathbf{u}_0 + \Delta\mathbf{u}) = (\lambda_0 + \Delta\lambda)\mathbf{f} \tag{15}$$

This is a system of N equations with $N+1$ unknowns. An additional constraint equation is defined as:

$$g(\mathbf{u}_0, \lambda_0, \Delta\mathbf{u}, \Delta\lambda, \kappa) = 0 \tag{16}$$

where κ is a parameter that defines the step size. This results in an augmented system of $N+1$ equations and $N+1$ unknowns:

$$\begin{bmatrix} \mathbf{f}_{\text{int}} \\ g \end{bmatrix} = \begin{bmatrix} \lambda\mathbf{f} \\ 0 \end{bmatrix} \tag{17}$$

which is solved with a Newton-Raphson iteration [9].

The constraint equation (16) is based on the rate of energy dissipation which is related to the damage evolution in a body and is strictly increasing when damage occurs [15]. However, when damage is not evolving, the rate of energy dissipation is zero and an alternative arc-length method has to be used. The rate of energy dissipation is equal to the exerted power P minus the rate of elastic energy $\dot{V}$:

$$G = P - \dot{V} \tag{18}$$

In a finite element context, the equilibrium equations (14) and constraint equation (16) are written in terms of nodal displacements $\underline{\mathbf{u}}$. The exerted power is then given by:

$$P = \mathbf{f}_{\text{ext}}^{\text{T}} \dot{\underline{\mathbf{u}}} = \lambda \mathbf{f}^{\text{T}} \dot{\underline{\mathbf{u}}} \tag{19}$$

The elastic energy depends on the constitutive behaviour of the material and kinematic formulation of the interface element. Unloading occurs along a path parallel to the elastic tangent and the elastic energy is given by:

$$V = \frac{1}{2}\int_{\Sigma} \mathbf{u}^{\text{e}\text{T}} \mathbf{t} d\Sigma = \frac{1}{2}\int_{\Sigma} \mathbf{t}^{\text{T}} \mathbf{K}^{\text{e}-1} \mathbf{t} d\Sigma \tag{20}$$

from which the rate of elastic energy is derived as:

$$\dot{V} = \int_\Sigma \dot{\mathbf{t}}^{\mathrm{T}} \mathbf{K}^{\mathrm{e}-1} \mathbf{t} d\Sigma = \int_\Sigma \dot{\mathbf{u}}^{\mathrm{T}} \mathbf{K}^{\mathrm{t}^{\mathrm{T}}} \mathbf{K}^{\mathrm{e}-1} \mathbf{t} d\Sigma = \dot{\underline{\mathbf{u}}}^{\mathrm{T}} \mathbf{f}^* \tag{21}$$

with

$$\mathbf{f}^* = \int_\Sigma \mathbf{B}^{\mathrm{T}} \mathbf{K}^{\mathrm{t}^{\mathrm{T}}} \mathbf{K}^{\mathrm{e}-1} \mathbf{t} d\Sigma \tag{22}$$

where the matrix $\mathbf{B}$ relates the nodal displacements $\underline{\mathbf{u}}$ to the local relative displacements $\mathbf{u}^{\mathrm{r}}$:

$$\mathbf{u}^{\mathrm{r}} = \mathbf{B}\underline{\mathbf{u}} \tag{23}$$

The energy release rate is rewritten as:

$$G = \dot{\underline{\mathbf{u}}}^{\mathrm{T}} (\lambda \mathbf{f} - \mathbf{f}^*) \tag{24}$$

The constraint equation for the arc-length method is obtained after a forward Euler time discretization:

$$g = \Delta \underline{\mathbf{u}}^{\mathrm{T}} (\lambda_0 \mathbf{f} - \mathbf{f}_0^*) - \kappa \tag{25}$$

4 EXAMPLES

Three numerical examples are performed. First, a direct tensile test and direct shear test are performed on a single interface element which are presented by Caballero et al. [3]. Afterwards, a direct shear test is performed on a small brick assembly.

4.1 Direct tension test

A first test consists of a direct tensile test on a single interface element (figure 2a) [3]. A normal displacement is applied to the nodes of the top face of the interface element while the bottom nodes are fixed. The normal and tangential elastic stiffness are $k_{\mathrm{n}} = k_{\mathrm{t}} = 1000\,\mathrm{MPa/mm}$. The parameters defining the initial yield and potential surface are listed in table 1.

Table 1: Interface parameters used in the direct tension test.

χ_0 [MPa]	c_0 [MPa]	$\tan\phi_0$ [-]	$\tan\phi_{\mathrm{r}}$ [-]	c_{g0} [MPa]	$\tan\phi_{g0}$ [-]	$\tan\phi_{g\mathrm{r}}$ [-]
3	14	0.8	0.2	45	0.04	0.04

The response of the interface is studied for different values of the fracture energy $G_{\mathrm{f}}^{\mathrm{I}} = 0.01,\ 0.02,\ 0.03,\ 0.05,\ 0.10\,\mathrm{N/mm}$, while $G_{\mathrm{f}}^{\mathrm{II}} = 0.10\,\mathrm{N/mm}$. Figure 3 shows the normal traction t_z in function of the normal relative displacement u_z^{r} for different fracture

energy values $G_{\mathrm{f}}^{\mathrm{I}}$. The interface behaves elastically until the initial tensile strength χ_0 is reached. The response curves are identical for the different values of $G_{\mathrm{f}}^{\mathrm{I}}$ up to the peak stress level. Afterwards, the response reduces exponentially with asymptotically vanishing normal traction. In case the fracture energy $G_{\mathrm{f}}^{\mathrm{I}}$ is low, the response reduces more rapidly then in case of a high fracture energy value. It follows from equation (3) that, for a tensile test, the area under the softening branch is equal to the fracture energy $G_{\mathrm{f}}^{\mathrm{I}}$. When the history value W^{p} reaches the fracture energy $G_{\mathrm{f}}^{\mathrm{I}}$, the tensile strength is zero and therefore, the increment of the history value dW^{p} in equation (3) is zero.

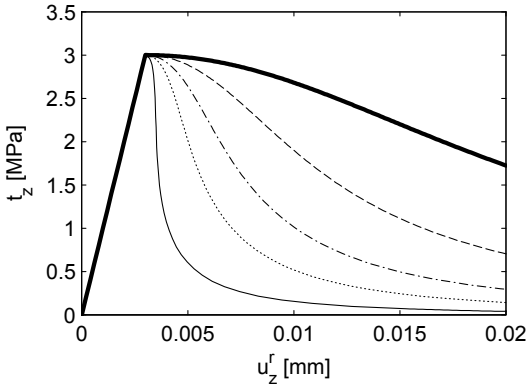

Figure 3: Normal traction t_z in function of relative normal displacement u_z^{r} for a fracture energy $G_{\mathrm{f}}^{\mathrm{I}} = 0.01$ (solid line), 0.02 (dotted line), 0.03 (dashed-dotted line), 0.05 (dashed line), 0.10 N/mm (thick solid line).

4.2 Direct shear test

In a second example a direct shear test is performed on a single interface element for different values of normal compression t_z [3]. In a first loading step, the interface element is loaded with a normal compressive stress t_z. Next, a shear force in the x-direction is applied at the top face while the bottom nodes remain fixed. The top nodes are kinematically constrained so that the rotation of the top face is prohibited. The test is repeated for different levels of constant normal traction ($t_z = -0.1$, -2.0, -6.0, -10.0 MPa). The normal and tangential elastic stiffness are $k_{\mathrm{n}} = k_{\mathrm{t}} = 25000\,\mathrm{MPa/mm}$. The parameters for the yield surface are listed in table 2. The fracture energy for mode I and mode II are respectively $G_{\mathrm{f}}^{\mathrm{I}} = 0.03\,\mathrm{N/mm}$ and $G_{\mathrm{f}}^{\mathrm{II}} = 0.06\,\mathrm{N/mm}$.

Figure 4a shows the shear traction t_x in function of the relative tangential displacement u_x^{r} for different compressive stresses. After the initial elastic response, the shear traction decreases for increasing shear displacement. Initially, in the steeper part of the softening branch, all softening parameters decrease until W^{p} reaches $G_{\mathrm{f}}^{\mathrm{I}}$ and the tensile capacity χ of the interface element reduces to zero. Next, W^{p} evolves to $G_{\mathrm{f}}^{\mathrm{II}}$ and the shear stress reduces to the residual value $\tau_{\mathrm{r}} = \sigma_z \tan\phi_{\mathrm{r}}$. The shear capacity of the interface increases

Table 2: Interface parameters used in the direct shear test.

χ_0 [MPa]	c_0 [MPa]	$\tan\phi_0$ [-]	$\tan\phi_\mathrm{r}$ [-]	c_{g0} [MPa]	$\tan\phi_{g0}$ [-]	$\tan\phi_{g\mathrm{r}}$ [-]
3	4.5	0.8785	0.2	45	0.04	0.04

with increasing confinement. Figure 4b shows the relative normal displacement u_z^r in function of the relative tangential displacement u_x^r. The dilatancy decreases for increasing confinement. Asymptotically, as the friction angle evolves to the residual friction angle, the dilatancy reduces and a smooth fracture surface is formed.

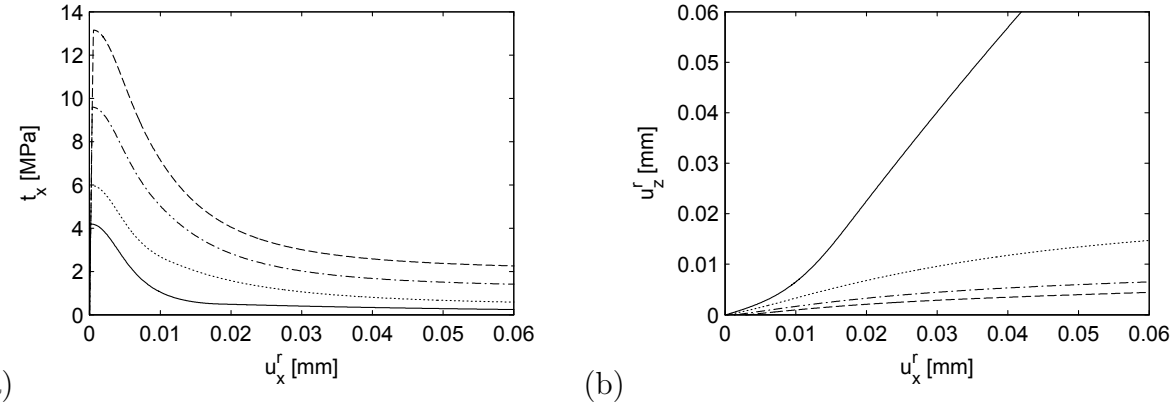

(a) (b)

Figure 4: (a) Shear traction t_x and (b) relative normal displacement u_z^r in function of the relative tangential displacement u_x^r for a normal traction $t_z = -0.1$ (solid line), -2.0 (dotted line), -6.0 (dashed-dotted line), $-10.0\,\mathrm{MPa}$ (dashed line).

4.3 2×1.5 brick wall

A small brick assembly, two bricks high and one and a half brick in length, is considered (figure 5a). Each brick measures $204 \times 98 \times 50\,\mathrm{mm}^3$. A shear test is performed on the assembly; in a first loading step, a vertical pressure $p_\mathrm{v} = 0.3\,\mathrm{MPa}$ is applied at the top face of the assembly, next a horizontal load F_h is applied at the top edge. The bottom face is fixed and the top face is kinematically constrained so that the rotations of the top face are prohibited. For the bricks, an elastic modulus $E_\mathrm{b} = 16700\,\mathrm{MPa}$ and a Poisson's ratio $\nu_\mathrm{b} = 0.25$ are assumed. Tables 3 and 4 show the mechanical properties for brick and brick-mortar interfaces used in the numerical analysis. These properties have also been used by Macorini et al. [4] to compare results from experimental tests on a masonry wall with numerical results obtained with a dynamic analysis.

The horizontal load F_h is applied in loading steps λF_h. Figure 6a shows the load-displacement curve where F_h is plotted in function of the horizontal displacement u_h

Table 3: Elastic properties interface elements.

	k_n [MPa/mm]	k_t [MPa/mm]
Mortar	82	36
Brick	10000	10000

Table 4: Mechanical properties interface elements.

	χ_0 [MPa]	c_0 [MPa]	$\tan\phi_0$ [-]	$\tan\phi_\mathrm{r}$ [-]	G_f^I]N/mm]	G_f^II [N/mm]	$c_{g,0}$ [MPa]	$\tan\phi_{g0}$ [-]	$\tan\phi_{g\mathrm{r}}$ [-]
Mortar	0.25	0.375	0.75	0.75	0.018	0.125	37.5	0.001	0.0001
Brick	2.0	2.8	1.0	1.0	0.08	0.5	2.8	1.0	1.0

of the top face of the segment. Initially, the segment behaves linearly and a standard arc-length procedure is used to obtain equilibrium. Before the peak load is reached, the central horizontal interface element starts yielding and the solution method switches to the dissipation based arc-length method. At the peak load, all horizontal interfaces are yielding and the softening behaviour of the interfaces is visible in the load displacement curve. The history variable W^p further increases for the three horizontal interface elements and reaches the fracture energy G_f^I. A bend in the load-displacement curve is observed at this point and the tensile strength of the interface elements reduces to zero (figure 6b). Figure 5b shows that a single horizontal crack is formed. The horizontal load further decreases and the yield surface of the horizontal interfaces evolves to a standard Mohr-Coulomb criterium with a tensile strength $\chi = 0\,\mathrm{MPa}$, cohesion $c = 0\,\mathrm{MPa}$ and friction angle $\tan\phi = 0.75$.

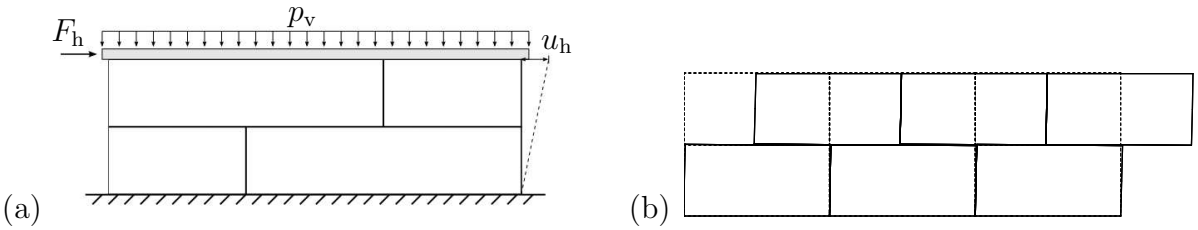

Figure 5: (a) 2×1.5 brick wall and (b) undeformed (dotted lines) and deformed mesh (solid lines) at the last loading step.

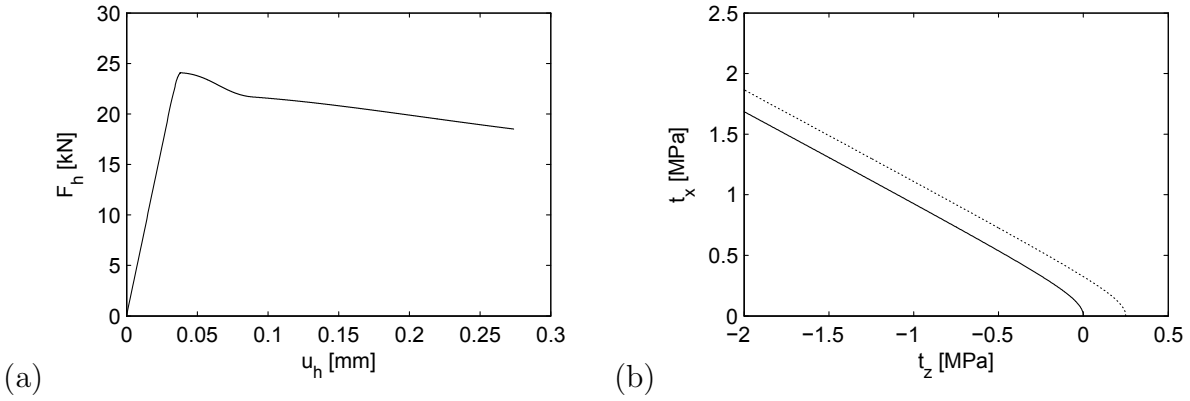

Figure 6: (a) Load-displacement curve and (b) initial (dotted line) and final yield surface (solid line).

5 CONCLUSION

A meso-scale model is used where masonry bricks are modelled using solid elements and the mortar layers are modelled using interface elements. It is assumed that cracks mainly propragate at the mortar joints and, therefore, a non-linear constitutive behaviour is presented for the interface element. An elasto-plastic contact law that follows a Mohr-Coulomb criterion is used to model failure in tension and shear.

The possible occurence of snapbacks during masonry cracking, that causes a sudden release of elastic energy, may result in numerical instabilities. Therefore, a dissipation based arc-length method is presented in which the constraint equation is based on the rate of energy dissipation which can be related to the propagation of damage in the structure.

A numerical test on a 2×1.5 brick wall indicates that the meso-scale model is suitable to model a small brick assembly, correctly capturing the failure process. However, when performing numerical tests on larger samples, the dissipation based arc-length method is not able to reach convergence after a number of loading steps. Currently, further research is in progress to enhance the dissipation based arc-length method with an efficient step size adjustment. Alternatively, an adaptive path following technique [10] and dynamic solution strategies are also considered.

REFERENCES

[1] P.B. Lourenço. *Computational strategies for masonry structures.* PhD thesis, Delft University of Technology, Delft, The Netherlands, 1996.

[2] P.B. Lourenço and J.G. Rots. A multisurface interface model for the analysis of masonry structures. *ASCE Journal of Engineering Mechanics*, 127(7):660–668, 1997.

[3] A. Caballero, K.J. Willam, and I. Carol. Consistent tangent formulation for 3D interface modeling of cracking/fracture in quasi-brittle materials. *Computer Methods*

in Applied Mechanics and Engineering, 197(33):2804–2822, 2008.

[4] L. Macorini and B.A. Izzudin. A non-linear interface element for 3D mesoscale analysis of brick-masonry structures. *International Journal for Numerical Methods in Engineering*, 85(12):1584–1608, 2011.

[5] R. Kumar, N.and Amirtham and M. Pandey. Plasticity based approach for failure modelling of unreinforced masonry. *Engineering Structures*, 80:40–52, 2014.

[6] M. Geers, V.G. Kouznetsova, and W.A.M. Brekelmans. Multi-scale computational homogenization: trends and challenges. *Journal of Computational and Applied Mathematics*, 234(7):2175–2182, 2010.

[7] L. Macorini and B.A. Izzuddin. Nonlinear analysis of unreinforced masonry walls under blast loading using mesoscale partitioned modeling. *ASCE Journal of Structural Engineering*, 140(8), 2014.

[8] M.A. Crisfield. A fast incremental/iterative solution procedure that handles snap-through. *Computers and Structures*, 13(1):55–62, 1981.

[9] C.V. Verhoosel, J.J.C. Remmers, and M.A. Gutiérrez. A dissipation-based arc-length method for robust simulation of brittle and ductile failure. *International Journal for Numerical Methods in Engineering*, 77(9):1290–1321, 2009.

[10] T. Pohl, E. Ramm, and M. Bischoff. Adaptive path following schemes for problems with softening. *Finite Elements in Analysis and Design*, 86:12–22, 2014.

[11] K. Krabbenhøft. Basic Computational Plasticity. *Lecture Notes*, 2002.

[12] I. Carol, P.C. Prat, and C.M. López. Normal/shear cracking model: application to discrete crack analysis. *ASCE Journal of Engineering Mechanics*, 123(8):765–773, 1997.

[13] K. Maekawa, H. Okamura, and A. Pimanmas. *Non-linear mechanics of reinforced concrete*. CRC Press, 2003.

[14] D. Dooms, G. De Roeck, G. Degrande, G. Lombaert, M. Schevenels, and S. François. StaBIL: A finite element toolbox for MATLAB. Technical Report BWM-2009-20, Department of Civil Engineering, KU Leuven, October 2009.

[15] M.A. Gutiérrez. Energy release control for numerical simulations of failure in quasi-brittle solids. *Communications in Numerical Methods in Engineering*, 20(1):19–29, 2004.